Energy as a Speed Mediation Mechanism for Lower-limb Exoskeleton-User Coordination

Lyndon Tang[1], Bhavya Giri Goswami[2], Atusa Ghorbani Siavashani[2], John McPhee[2], Rezvan Nasiri[1], Arash Arami[1,3] *Member, IEEE*

***Abstract*— The Velocity Flow Field (VFF) lower-limb exoskeleton controller is widely applicable for gait rehabilitation because it provides the user with considerable agency over their gait, however, mathematical analysis reveals a viscous damping behaviour that may interfere with the user's efforts. A corrected controller with an adaptation law is proposed that synchronizes the speed parameter by minimizing the average mechanical work transferred between the user and exoskeleton per step. Experiments comparing a fixed and adaptive controller with 12 participants walking at $40 \pm 10\%$ body length/s on a treadmill showed that the adaptive controller tracks changes in walking speed, while reducing the energy transferred by the fixed controller from -0.541 ± 0.126 $\frac{J}{\text{step}}$ absorbed from the user to 0.0484 ± 0.0117 $\frac{J}{\text{step}}$ supplied for the adaptive controller at the fastest speed. Analysis of the human-exoskeleton interaction portrait showed that for most participants, the adaptive controller at medium and fast speeds substantially reduced user-controller disagreement, and increased user agency over the walking motion. These positive results motivate the optimization of the energy supplied per step as a viable mechanism for coordinating a personalized, real-time-adjusted walking speed between the user and the exoskeleton.**

I. Introduction

Gait training is a therapeutic intervention for incomplete spinal cord injury focused on redeveloping locomotor ability. In this context, lower-limb exoskeletons are a promising tool that provide controlled sensory and muscular experiences that promote motor learning and adaptation [1], [2], while compensating for deficits in strength and control and enabling longer, repeatable, and measurable walking training [3]. To this end, various control strategies have been proposed to achieve the desired rehabilitation outcomes. Feedforward assistive controllers are a simple way to provide repeatable, baseline assistance that supports the user in achieving the desired task. The actions of the exoskeleton may be triggered by gait cycle events, neuromuscular signals, or temporal synchronization signals [3], [4]; however, they may fail to achieve synchronicity with the user since they do not consider the user's ongoing efforts to accomplish the task in collaboration with the exoskeleton.

In order to achieve more cohesive synchronization with the user, impedance-based control strategies operate so that the exoskeleton intervenes when the user deviates from a desired trajectory, and otherwise behaves passively, by means of virtual mechanical impedance, channels, and static force fields [3], [4]. This second control approach is often referred to as the assist-as-needed paradigm. This is achieved through various techniques such as dead-zones [5], variable impedance control [6], optimal control within desired dynamical and kinematic constraints (i.e. control barrier functions) [7], and static force fields [8]. The effectiveness of these designs relies on the successful coordination between the intended movements of the user and the exoskeleton, which is negotiated through the sensory and actuation mechanisms of both agents. Coordination of the exoskeleton with the user requires the exoskeleton to alter its behaviour and adjust to the abilities and unique tendencies of the user.

The Velocity Flow Field (VFF) controller is an assist-as-needed controller which uses a velocity field in hip-knee joint space that coerces the user towards and along a desired trajectory [8], [9]. Its simple control law provides users with substantive agency over their gait, however, studies have shown that poorly tuned parameters can lead to a decreased range of motion and viscous damping behaviour that feels like walking through water [**?**].

In this study, the VFF controller was mathematically analyzed to show that the control law can be decomposed as the sum of purely corrective and assistive components, resulting in two novel contributions 1) an explanation and correction for the viscous damping effect that can inhibit the best efforts of the user. 2) A novel auto-tuning method for a modified VFF controller that achieves dynamic synchronization of speed and strength of assistance with the user across changes in walking speeds.

II. Background

A. Analysis of the VFF Control Law

The VFF control law defines a time-invariant velocity field in the hip-knee joint space that flows towards a predefined reference path, corresponding to the typical hip and knee flexion trajectories during the swing phase of a gait cycle [8]. The flow control torque law is defined as

$$\tau = C_d(\omega_{ref} - \omega) \tag{1}$$

This research was funded in part by NSERC Discovery grant number RGPIN-2024-06873, and in part by the New Frontiers in Research Fund-Exploration grant number NFRFE2022-620.

[1]Lyndon Tang and Arash Arami are with the Department of Mechanical and Mechatronics Engineering, University of Waterloo, Waterloo, ON, N2L 3G1, Canada le2tang@uwaterloo.ca; arash.arami@uwaterloo.ca

[2]Bhavya Giri Goswami, Atusa Ghorbani Siavashani, and John McPhee are with the Department of System Design Engineering, University of Waterloo, Waterloo, ON, N2L 3G1, Canada b4goswam@uwaterloo.ca; a9ghorba@uwaterloo.ca; mcphee@uwaterloo.ca

[3]Arash Arami is also with KITE Institute, Toronto Rehabilitation Institute, University Health Network, Toronto, ON M5G 2A2, Canada.

**Corresponding author: Arash Arami.*

where $C_d = 0.016$ is the drag coefficient, $\omega \in \mathbb{R}^2$ is the vector of hip and knee flexion angular velocities. The reference velocity, $\omega_{ref} \in \mathbb{R}^2$, is a unit vector, $\nu \in \mathcal{S}^1$, scaled by the *nominal path speed*, $\Gamma \in \mathbb{R}_+$.

$$\omega_{ref} = \Gamma\nu \tag{2a}$$

$$\nu = \frac{\|\mathbf{e}\|^2}{\sqrt{\|\mathbf{e}\|^4 + k_{sh}^2}}\mathbf{n} + \frac{k_{sh}}{\sqrt{\|\mathbf{e}\|^4 + k_{sh}^2}}\mathbf{t} \tag{2b}$$

$$= \sigma(\mathbf{e})\mathbf{n} + \bar{\sigma}(\mathbf{e})\mathbf{t} \tag{2c}$$

where $\mathbf{e} = \mathbf{q}_{ref} - \mathbf{q} \in \mathbb{R}^2$ is the *path error*, which is the vector between the current hip-knee joint configuration, $\mathbf{q} \in \mathbb{R}^2$, and the nearest joint configuration on the reference path, $\mathbf{q}_{ref} \in \mathbb{R}^2$, $\mathbf{n} \in \mathcal{S}^1$ is the unit vector in the direction of the error, and $\mathbf{t} \in \mathcal{S}^1$ is the unit vector tangent to the reference path at the nearest reference joint configuration, in the direction of motion during a typical gait cycle. The shape parameter, $k_{sh} = 16$ is defined in [8].

For notational convenience, the scaling factors, $\sigma(\mathbf{e}) \in [0, 1)$ and $\bar{\sigma}(\mathbf{e}) \in (0, 1]$ are defined such that $\|\nu\| = \sqrt{\sigma^2(\mathbf{e}) + \bar{\sigma}^2(\mathbf{e})} = 1$. The normal and tangential components of the reference velocity are inversely coupled by this constraint so that when $\|\mathbf{e}\| \geq \sqrt{k_{sh}}$, with equality marking the crossover point, the normal (corrective) component starts dominating.

Substituting Eq.2 into Eq.1 and rearranging gives

$$\tau = \underbrace{C_d\Gamma\sigma(\mathbf{e})\mathbf{n}}_{\tau_c} + \underbrace{C_d(\Gamma\bar{\sigma}(\mathbf{e})\mathbf{t} - \omega)}_{\tau_a} \tag{3}$$

The control law can be decomposed into two interpretable components. The *corrective torque*, $\tau_c \in \mathbb{R}^2$, is entirely dependent on the path error, bounded in magnitude between $[0, C_d\Gamma)$, and redirects the user's joint configuration towards the reference path. The *assistive torque*, $\tau_a \in \mathbb{R}^2$ propels the user along the path with the reference velocity. In the extreme cases, large error causes $\nu \simeq \mathbf{n}$, meaning the control is dominated by corrective torques and the objective is to bring the user closer to the reference path. On the other hand, small error causes $\nu = \mathbf{t}$, so the assistive torques dominate, and the control objective is to regulate the joint velocities to the *nominal path velocity*, $\dot{\mathbf{q}}_{ref} = \Gamma\mathbf{t} \in \mathbb{R}^2$, which is in the tangent direction with a magnitude of the nominal path speed.

A subtle problem in the original control law, evident from the expression for τ_a, is that when the error is large, $\tau_a \simeq -C_d\omega$ behaves like a viscous damper. Consequently, if the reference trajectory is poorly tuned for the user, the controller consistently resists the user's movements, which results in a continuous loss of energy from the user and a feeling of walking through water.

B. User-Controller Agreement and Energy Transfer

The power supplied by the exoskeleton at a joint can be formulated by $P = \tau\omega \in \mathbb{R}$. If the motor torque and joint velocity have the same sign, the exoskeleton supplies power to the system; if they have opposite signs, it absorbs power from the system. Thus, the sign of power indicates whether the exoskeleton assists or opposes the motion. The work done by the exoskeleton (i.e., the total mechanical work exchanged), during each step, is the time integral of power:

$$E_{step} = \int_{T_{step}} (\tau^T\omega)dt \tag{4}$$

and is one of the indicators of the overall coordination between the exoskeleton and user [10], [11]. If the exoskeleton is constantly absorbing energy from the user, then, on average, the mechanical work is negative and the exoskeleton is opposing motion more than it encourages. In [**?**], large negative energy values caused crouch walking and shuffling. On the other hand, positive values were associated with a perception of jittery, unstable motion, and large pushes from the exoskeleton. Thus, ideally the exoskeleton power contribution should not be negative nor highly positive.

C. User-Controller Interaction Portraits

The sign of power is a reliable measure of user–controller agreement, but it does not incorporate any direct measurement from the user. A recent study proposed a novel evaluation framework, called the interaction portrait (IP), for qualitatively assessing user–controller interaction [12]. IP is a visual framework that compares the change of muscular effort and the magnitude of interaction torques (torques exerted by the user on the exoskeleton) between two controllers as a two-dimensional variable. According to [12], when both the muscular effort and interaction torques change with the same sign, there is an increase (both positive) or decrease (both negative) in the disagreement between the exoskeleton and user's intentions. On the other hand, when the interaction torques decrease but the muscle effort increases, the user takes control over the exoskeleton, whereas an increase in interaction torques with decreased muscle effort shows the user yields control to the exoskeleton.

III. METHODS

In this section, modifications to the original VFF controller, along with a novel adaptive algorithm that uses energy transfer to autonomously tune the nominal path speed of the controller are shown. The experimental protocol conducted to compare fixed and adaptive versions of the controllers is then shown.

A. Modified VFF Control Law

Three modifications were made to the assistive component of the original control law in Eq.(3).

First, given the separate roles of the corrective and assistive torques and the different roles that Γ plays in each component, two distinct parameters Γ_c and Γ_a were assigned for the corrective and assistive components, respectively.

In accordance with the assist-as-needed paradigm, $\Gamma_c = 266\ ^\circ/s$ was set to a constant value, corresponding to the average path speed observed from a representative participant walking at medium speed ($40\ \%BL/s$), which is the proposed value in [**?**], to assert that the desired kinematic pattern is always pursued.

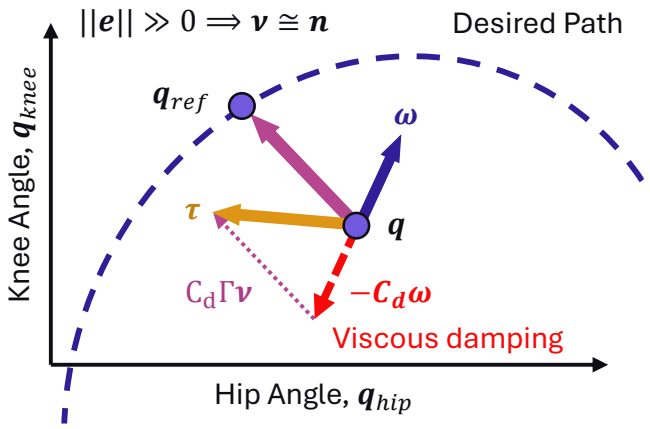

Fig. 1. The original control law torque (yellow) comprises of a corrective (pink) and viscous damping term (red) when the current joint configuration is far from the desired path, in this case resisting knee flexion and hip extension of the swing leg.

In the assistive torques, Γ_a is the desired speed along the reference path under ideal zero-error conditions; thus, the parameter was augmented to vary along the path so that the reference joint velocities match the kinematic trajectories during normal, unassisted walking, which indeed vary significantly over the gait cycle [**?**]. The nominal path velocity was replaced with $\dot{\mathbf{q}}_{ref}(\theta) : [0, 1) \to \mathbb{R}^2$, a fixed, parametric function of the normalized step time, $\theta \in [0, 1)$, fit to the typical joint velocities during unassisted walking at $40\%BL/s$ with least squares regression. A scaling factor, $\gamma_a \in \mathbb{R}_+$, then modulates the nominal joint velocities to control the desired speed of the walking gait. This is equivalently interpreted as using a phase-varying $\Gamma_a = \gamma_a \|\dot{\mathbf{q}}_{ref}(\theta)\|$ since the tangent direction can be expressed as $\mathbf{t} = \frac{\dot{\mathbf{q}}_{ref}}{\|\dot{\mathbf{q}}_{ref}\|}$ [**?**].

The next modification aimed to resolve the viscous damping behaviour that emerges when the path error is large as shown in Fig.1. The user's current joint velocity, ω was decomposed into normal and tangential components, $\omega_n = \text{proj}_n(\omega)$, $\omega_t = \text{proj}_t(\omega) \in \mathbb{R}^2$. The damping behavior was mitigated by gating the tangential component of the user's current angular velocity by $\bar{\sigma}(\mathbf{e})$. Consequently, in high error cases, no damping occurs along the path due to the $-C_d\omega_t$ term, and in low error cases, the speed along the path is regulated so that ω converges to $\gamma_a\dot{\mathbf{q}}_{ref}$. For notational convenience, let $\omega_{\bar{\sigma}} = \omega_n + \bar{\sigma}(\mathbf{e})\omega_t \in \mathbb{R}^2$ be the *tangentially gated joint velocities*.

Lastly, the estimated Coriolis and gravitational torques of the exoskeleton, $H_e = \hat{h}_e(\mathbf{q}, \dot{\mathbf{q}})$, were added to compensate for the inertia. Thus, the modified controller was given by:

$$\tau = \underbrace{C_d\left[\Gamma_c\sigma(\mathbf{e})\mathbf{n} - \omega_n\right]}_{\tau_c} + \underbrace{C_d\bar{\sigma}(\mathbf{e})\left[\gamma_a\dot{\mathbf{q}}_{ref} - \omega_t\right]}_{\tau_a} + H_e \quad (5)$$

B. Adaptive Nominal Path Speed Tuning

When the path error is small, which is asserted by the corrective torques, then $\bar{\sigma}(\mathbf{e}) \simeq 1$, and the sign of the assistive torque in Eq.(5) depends on the signs of the hip and knee elements of $\gamma_a\dot{\mathbf{q}}_{ref} - \omega$. Consequentially, assistance is applied and power is supplied if the reference velocity is higher than the user's, whereas resistance is given and power is absorbed if the reference velocity is lower than the user's. This principle is used to automatically select the minimal level of assistance that does not result in dissipative behavior through an autonomous adaptation law that selects γ_a.

The power transferred by the exoskeleton due to the control law is,

$$P = \left[C_d\Gamma_c\sigma(\mathbf{e})\mathbf{n} + C_d(\gamma_a\bar{\sigma}(\mathbf{e})\dot{\mathbf{q}}_{ref} - \omega_{\bar{\sigma}})\right]^T\omega \quad (6)$$

The linear form of the dot product allows us to decompose the power into the corrective and assistive components.

$$P_c = C_d\Gamma_c\sigma(\mathbf{e})\mathbf{n}^T\omega \quad (7a)$$

$$P_a = C_d\gamma_a\bar{\sigma}(\mathbf{e})\dot{\mathbf{q}}_{ref}^T\omega - C_d\omega_{\bar{\sigma}}^T\omega \quad (7b)$$

The power supplied by the exoskeleton due to the assistive torque is linear with respect to γ_a, thus, the energy supplied by the exoskeleton is as well.

$$E_a = \gamma_a\int_{T_{step}}\left[C_d\bar{\sigma}(\mathbf{e})\dot{\mathbf{q}}_{ref}^T\omega\right]dt - \int_{T_{step}}\left[C_d\omega_{\bar{\sigma}}^T\omega\right]dt \quad (8)$$

For notational simplicity, the scale and bias terms in Eq.(8) are defined as

$$a = \int_{T_{step}}\left[C_d\bar{\sigma}(\mathbf{e})\dot{\mathbf{q}}_{ref}^T\omega\right]dt \quad (9a)$$

$$b = -\int_{T_{step}}\left[C_d\omega_{\bar{\sigma}}^T\omega\right]dt \quad (9b)$$

The adaptation objective is to choose γ_a such that the assistive work done by the exoskeleton is zero. This is equivalent to minimizing the cost function $J(\gamma_a) = \frac{1}{2}(a\gamma_a + b)^2$ while keeping γ_a positive and bounded within a predefined maximum value ($\bar{\gamma}_a$) to avoid excessive, uncomfortable torques being applied to the user.

$$\begin{aligned}\arg\min_{\gamma_a} \quad & \frac{1}{2}(a\gamma_a + b)^2 \\ \text{s.t.} \quad & 0 \le \gamma_a \le \bar{\gamma}_a\end{aligned} \quad (10)$$

Since E_a depends on the user's energy contribution to the system, through changes in the joint velocities, and the user's behavior is widely varying across individuals and time-varying based on the user's intent, the objective function is quasi-static. An online Accelerated Projected Gradient Descent (APGD) was used to continually solve the constrained optimization problem for γ_a [13], [14]. In Algorithm-1), the projection operator, $P : \mathbb{R} \to \mathbb{R}$ is the saturation operation, and $\alpha, \beta \in \mathbb{R}_+$ are the momentum factor and learning rate, respectively. The learning rate was $\beta = 0.05$ and the update frequency of γ_a was $0.5\ Hz$ to allow the user to feel the change in torques over the next step and make adjustments for the next step.

Algorithm 1 Accelerated Projected Gradient Descent Step

Input: $\gamma_a[k], k \geq 0$
Output: $\gamma_a[k+1]$

function UPDATE STEP($\gamma_a[k]$)
  $\hat{a}[k] \leftarrow \int_{T_k}(C_d\bar{\sigma}(\mathbf{e})\dot{\mathbf{q}}_{ref}^T\omega)dt$
  $\hat{b}[k] \leftarrow -\int_{T_k}(C_d\omega_\sigma^T\omega)dt$
  $\alpha[k] \leftarrow \frac{k-2}{k+1}$
  $y[k+1] \leftarrow \gamma_a[k] + \alpha(\gamma_a[k] - \gamma_a[k-1])$
  $\nabla_{\gamma_a}J(y[k+1]) \leftarrow a[k](a[k]y[k+1] + b[k])$
  $\gamma_a[k+1] \leftarrow \mathrm{P}(\gamma[k] - \beta\nabla_{\gamma_a}J(y[k+1]))$
  return $\gamma_a[k+1]$
end function

C. Experimental Protocol and Evaluation

The proposed auto-tuning method was evaluated by comparing a controller with an adaptive value of γ_a (*adaptive controller*) to a version with a fixed $\gamma_a = 1$ (*fixed controller*) with on an Indego Explorer exoskeleton (Ekso Bionics, USA), at slow, medium, and fast walking speeds on an instrumented treadmill (Bertec, USA), corresponding to 30%, 40%, and 50% of the participants' body length per second.

Twelve participants (6 male, 6 female, age: 26 ± 4 $years$, body mass: 69.5 ± 21.3 kg, height 1.71 ± 0.06 m, mean $\pm$ std) with no known neuromuscular impairment participated in the study. The participants provided informed consent prior to the experiment. The study protocol was conducted in accordance with the Declaration of Helsinki and reviewed and approved by the University of Waterloo Research Ethics Board (ORE#41794).

The trial, shown in Fig.2B, was composed of two sections corresponding to the fixed and adaptive controllers. Participants were randomly assigned the order in which they experienced the fixed or adaptive controller. Each section started with a calibration period, where the participant walked at 40 $\%BL/s$ for $30s$ with compensation for the exoskeleton inertial dynamics and no VFF controller. The reference path for the participant was fit to the average hip and knee flexion angle and velocity trajectories, using an online least squares algorithm, during the last twenty seconds of the calibration period. The section then proceeded with three conditions of steady-state walking at 30%, 40%, 50 $\%BL/s$ for ninety seconds each, followed by a linear ramp down from $50-30$ $\%BL/s$ over forty-five seconds, then back up. The period where the speed ramped down and up is called the dynamic condition. Given the heights of the participants, the average slow, medium, and fast treadmill speeds were 0.514 ± 0.019 $m/s, 0.685 \pm 0.026$ $m/s, 0.856 \pm 0.032$ m/s. Participants were asked to rate the feeling of disagreement between them and the exoskeleton during each condition, and choose their preferred controller in the end as part of the questionnaire.

The embedded joint encoder sensors in the exoskeleton were used to measure the joint angles and velocities at a sampling rate of 200 Hz. Retro-reflective motion capture

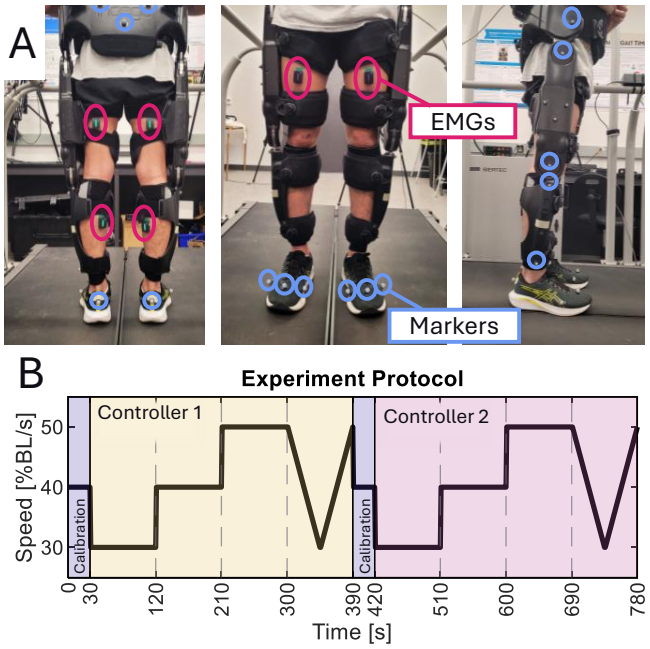

Fig. 2. A) Muscle activities are measured with surface electromyography sensors (pink), while kinematics are measured with retroreflective motion capture markers (blue) and exoskeleton joint encoders. B) Experiment protocol is composed of two sections, one for each fixed and adaptive controllers (randomized order).

markers were used on the heel, as well as the first, third, and fifth metatarsal (MP) joints of each foot to record the kinematics of the feet downsampled from 2000 Hz to 200 Hz as shown in Fig.2A. Muscle activities were measured with surface electromyography (EMG) sensors (Trigno, Delsys, USA) placed on the Rectus Femoris (RF), long head of the Biceps Femoris (BF), and medial head of the Gastrocnemius (GM) at a sampling frequency of 2000 Hz. EMG signals were bandpass filtered to $10-450$ Hz with a fourth order Butterworth filter, followed by full-wave rectification and smoothing with a fourth-order 8 Hz Butterworth filter. The EMG data was then downsampled to 200 Hz before normalization to the maximum EMG value observed over the whole trial for each participant. Human-exoskeleton interaction torques at each joint were estimated with the neural network method proposed in [15] that converts time-delayed measurements of joint kinematics to interaction torques.

To build the interaction portraits, muscle effort, which is the integral of the squared muscle activities over every step, was calculated for each of the RF, BF, and GM, and weighted averaged with weights were the physiological cross-sectional area (PCSA) of the muscles (RF: 13.5, BF: 10.8, GM: 21.0) which are proportional to maximum muscle force [16], [12]. The normalized interaction torques were computed by summing the integral of the absolute value of the estimated interaction torques of the hip and knee joints, normalized by the maximum amplitude in each trial. The values of the adaptive controller were centered and scaled around the average values from the fixed controller and plotted on a two-dimensional axis, with the difference in torque magnitudes

along the x-axis, and the difference in muscle effort along the y-axis.

The average path error and *path speed* (Euclidean norm of the hip-knee joint error and velocity, respectively), joint ranges of motion, and power trajectories were computed for the participant's dominant leg. Spatiotemporal gait metrics, such as the maximum height of the foot above the ground during the swing phase (peak foot clearance), the step duration, and the stride length were computed from the foot marker trajectories. In the steady-state conditions, the average step metrics were computed, including data from the last forty-five seconds of each condition.

A 4-group Friedman test with significance level of $\alpha = 0.05$ was used to evaluate group-level differences in the average statistics for each participant between the fixed and adaptive controllers. A post-hoc Wilcoxon signed-rank test with $\alpha = 0.05$ and Bonferroni correction was then used to analyze differences at each speed.

IV. Results

In this section, the performance of the adaptive controller is compared to the fixed controller based on assistive energy transferred by the exoskeleton, spatiotemporal gait metrics, as well as the user's behavior through interaction portraits and average muscle activation. Numerical results are presented as mean $\pm$ standard error of the mean.

A. Energy and Power Transfer

The Friedman test comparing energy supplied by the assistive torques showed significant differences between the fixed and adaptive controllers ($p << 0.001$). The Wilcoxon Signed Rank test further confirmed that, at medium, fast, and dynamic speeds, the energy supplied by assistive torques was significantly higher for the adaptive controller, compared to the fixed version (medium, fast, dynamic all $p =< 0.001$). There was no significant difference between the two controllers at the slow speed ($p = 0.677$).

The energy absorbed by the fixed controller per step increased, from an average of -0.0466 ± 0.0969 $\frac{J}{\text{step}}$ at slow speed to -0.541 ± 0.125 $\frac{J}{\text{step}}$, and -0.376 ± 0.108 $\frac{J}{\text{step}}$ at medium and fast speeds, and -0.376 ± 0.108 $\frac{J}{\text{step}}$ during the dynamic condition. In contrast, the average energy transferred by the adaptive assistive torques per step was much smaller in magnitude with lower variance with 0.00701 ± 0.0119 $\frac{J}{\text{step}}$, 0.0286 ± 0.0136 $\frac{J}{\text{step}}$, and 0.0484 ± 0.0117 $\frac{J}{\text{step}}$ for slow, medium, and fast speeds, respectively.

The top row of Fig.3B shows the progression of adaptation of γ_a as the walking speed changes for a representative participant. For each of the steady-state speeds, the initial reference velocity starts with a scale of 1, and changes to keep the energy supplied per step (bottom row), close to zero. In the slow speed, the scaling factor reduced to a minimum value of 0.910 and a final value of 0.954, while in the medium speed, the scaling factor peaked at 1.07 and ended at 1.03, and for the fast speed, peaked at 1.19 and ended at 1.16.

In the dynamic condition, the scaling factor starts at the last value in the fast walking condition, ($\gamma_a = 1.09$) and as the treadmill speed ramps down, the assistive energy of the adaptive controller is positive, indicating that the exoskeleton is supplying surplus energy, causing γ_a to drop. Once the treadmill ramps back up, so does γ_a (following a delay of 8 steps).

B. Controller Regulation Objectives

The adaptive controller did not result in any significant changes in corrective behaviour, compared to the fixed controller, as expected. The Friedman test comparing both the controllers did not show any significant differences in the RMSE ($p = 0.175$), peak foot clearance ($p = 0.773$), range of motion of the hip ($p = 0.273$) and knee ($p = 0.525$), step duration ($p = 0.954$), nor the stride length ($p = 0.977$), as expected since the two controllers share the same corrective control components.

Fig.5A shows that across all participants, the average RMSE per step is reasonable. The median RMSE is at worst $6.08 \pm 0.38°$ and $5.49 \pm 0.38°$ during the fast walking condition for both controllers.

The spatiotemporal gait metrics measured in this experiment, align well with expected values found in the literature of kinematics around the same speeds [17]. During the dynamic walking condition, which covers all speeds, the average peak foot clearance was 21.9 ± 0.5 cm for the fixed and 22.0 ± 0.6 cm for the adaptive controller. The ranges of motion for the hip and knee were 40.1 ± 1.3 ° and 39.5 ± 1.2 ° for the fixed controller, or 39.5 ± 1.2 ° and 47.4 ± 3.1 ° for the adaptive controller. The step duration for the fixed controller increased from 1.60 ± 0.06 s at the slow speed to 1.26 ± 0.04 s at the fast speed, and from 1.58 ± 0.05 s to 1.29 ± 0.04 s for the adaptive controller. The stride length for the fixed controller varied between 0.794 ± 0.028 m and 1.05 ± 0.03 m in the slow and fast speeds, while the adaptive controller resulted in stride lengths between 0.784 ± 0.026 m at slow speed to 1.08 ± 0.03 m.

C. Interaction Portrait and Muscle Activation

The IP plot in Fig.6A compares the average muscular effort and interaction torques of all participants during the last 20 seconds of the adaptive controller with those of the fixed controller. At the slow speed, most participants took control of the exoskeleton (second quadrant) or let the exoskeleton lead (fourth quadrant). At medium and fast speeds, most participants ended with less user-controller disagreement (third quadrant) for the adaptive controller.

To show the progression of user-exoskeleton interaction, Fig.6B shows the change in interaction over time for a representative participant with respect to the average interaction observed for the fixed controller. For all three speeds, the adaptive interaction points trend mostly towards the second and third quadrants, corresponding to decreased interaction torques.

Fig.7 compares the difference in the PCSA-weighted average muscle activation between controllers for each participant. Positive changes correspond to increased muscle

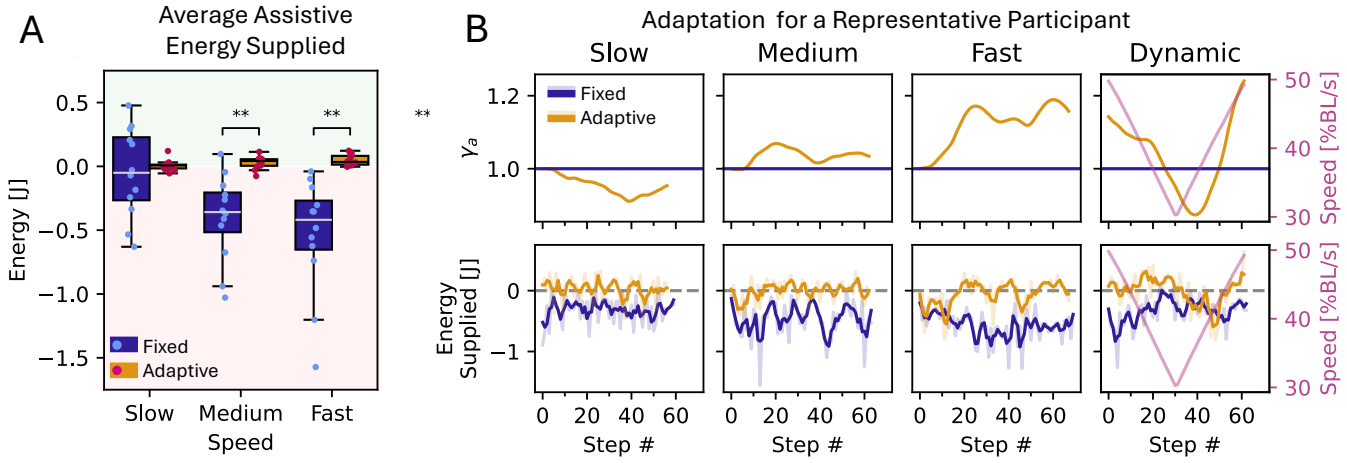

Fig. 3. A) Average energy supplied by assistive torques per step across all participants. B) Value of the nominal path speed scaling factor (top) adapts to changes in the walking speed for a representative participant, causing the energy supplied per step by assistive torques (bottom) to stay close to zero even though the speed changes. The three-step average is overlaid on the instantaneous energy per step in reduced opacity.

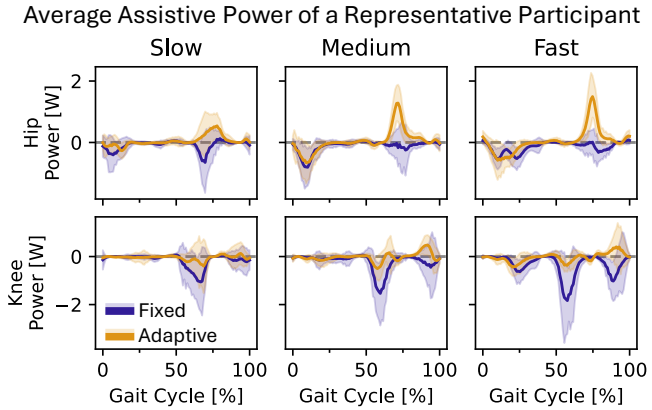

Fig. 4. The mean trajectory with unit standard deviation confidence intervals of power supplied to the hip (top) and knee (bottom) joints by the assistive torques for a representative participant.

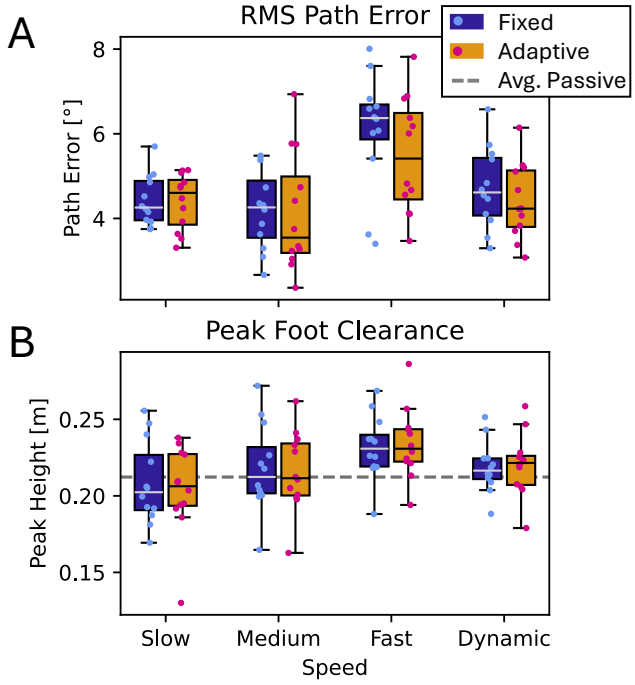

Fig. 5. A) Participant average path tracking error. B) Average peak height of the foot above the ground.

activations with the adaptive controller, and negative values indicate decreases in activation with respect to the average with the fixed controller. While the Friedman test did not yield significant results ($p = 0.341$), more than 75% of participants had a higher average muscle activation level during walking with the fixed controller in medium, fast, and dynamic speed conditions. At the fast and dynamic speeds, reductions in muscle activation were as large as 5% for several participants.

V. Discussion

A. Modifications to the Original Flow Controller

The viscous damping behavior for large error scenarios in the original control law, explained in Fig.1, leads to power dissipation and fast fatigue as shown in Fig.3, where the average assistive energy was typically negative for the fixed controller at the medium and fast speeds, requiring the user to exert more effort. This is justifiable for certain cases in rehabilitation, when the user cannot establish a safe gait pattern on their own, so the desired behavior is to halt user error and prioritize correction before continuing the motion. However, this damping behavior can also become obstructive when the desired path is not well tuned to the user's anthropometric variations or preferred walking speeds which may be highly variable across users [18], [19]. Obstruction is particularly evident when the knee flexion angle of the swing leg is substantially lower than the desired value given the hip flexion angle, the scenario in Fig.1. The large path error causes the controller to act like a viscous damper along the direction of step progression. The resulting resistance,

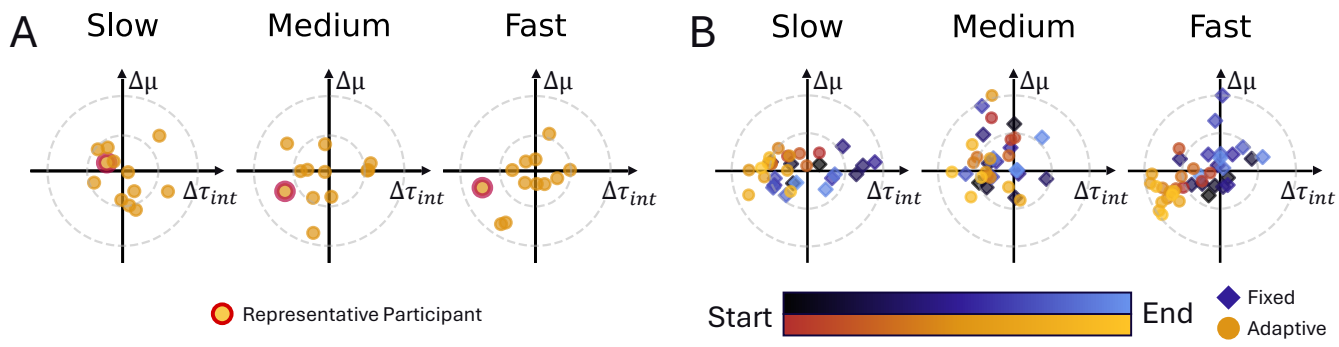

Fig. 6. A) Average difference in interaction between the last 20 s of the adaptive controller with respect to the last 20 s of the fixed controller for each participant. B) Temporal progression IPs of the representative participant highlighted in A, comparing every 4 steps of each controller with respect to the mean interaction value of the fixed controller over all points. Brighter points correspond to later steps.

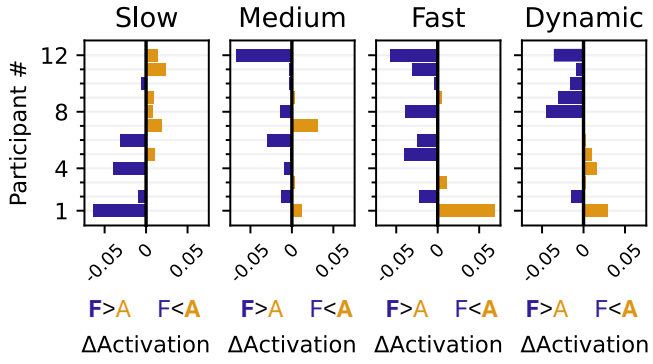

Fig. 7. Difference in the average muscle activation between the adaptive and fixed controllers for each participant.

applied while the user is in an unstable position, inhibits further knee flexion and hip extension. This reduces the overall range of knee flexion and foot clearance, increasing the risk of stumbling or falling, and worsens tracking error, thereby reinforcing unwanted behavior.

The proposed control law, Eq.(5), does not inhibit users in their current motion, even if the error is very large. The $\bar{\sigma}(e)$ in Eq.(5) collapses the assistive torques to zero, leaving only the corrective torques in the normal direction and no resistance in the tangential direction, allowing the user to converge more smoothly towards the desired path.

In the dynamic condition, γ_a tracks the changes in treadmill speed in Fig.3B demonstrating that the adaptive controller correctly reduces assistance when over-assisting at a slower speed, and synchronizes with the user when they exert more energy to speed up.

The learning rate, β, and update frequency in Algorithm(1) were chosen in the pilot experiments. Choosing update frequencies faster than $0.7\ Hz$ or learning rates $\beta > 0.1$ led to large changes in γ_a between consecutive steps, leading to oscillating changes in both user and exoskeleton behaviour in consecutive steps. The iterative APGD solver requires a consistent optimization problem between iterations to converge to a solution, meaning the user's behaviour must be quasi-static, which requires slow adaptation. The oscillations in the adaptive γ_a in the last 20 steps of the steady state conditions in Fig. 3B shows the unavoidable co-adaptation of the user to changes in the joint torques under otherwise constant conditions. Effectively, this suggests that a limiting factor preventing faster adaptation rates is the maximum rate in which the user can interpret, anticipate, and react to changes in the behaviour of the exoskeleton.

B. User-exoskeleton Interaction and Feedback

Both the participant average and representative IPs in Fig. 6 show that for all three speeds, the adaptive controller outperforms the fixed version by reducing interaction torques, thereby enhancing user-controller agreement and allowing the user to exercise agency without disagreement. Furthermore, in Fig.6B, the shift of adaptive controller points towards the third quadrant across all speed conditions indicates that the adaptive controller progressively increased user-controller agreement over time.

In the questionnaire, 8 out of 12 participants preferred the adaptive controller and reported experiencing less resistance when walking, particularly at medium and fast speeds. Those who favored the fixed controller felt that the adaptive controller moved them along a different kinematic path from what they wanted. Furthermore, they liked the stronger sense of assistance at slow speeds with the fixed controller, which emerges since the fixed controller was tuned for the medium speed, causing positive assistive energy for slow speed as also shown in Fig.3A. This difference in preference is reflected in the muscle activity in Fig. 7, where certain participants had substantial decreases in muscle activity across all speeds, while others had increases.

C. Limitations

The adaptive controller helps users to track a desired reference trajectory with minimal assistance, however, users with severe ambulatory deficits may find it impossible to make movements that further step progress when the assistance provided by the controller is minimal. A tunable bias can be added to the cost function in Eq.(10), modifying the objective

of the adaptation law to drive the mechanical work to a positive setpoint value, so that the user always experiences a baseline level of assistance. The encouraging results in this study, demonstrating regulation of the mechanical work due to assistive torque, suggest that the work is indeed controllable to reach and hold an arbitrary setpoint.

This study focused on treadmill walking, although the adaptive controller is expected to have a greater application in overground walking. Varying conditions in overground locomotion were simulated by changes in treadmill speed, yet, real-world walking involves frequent and varied changes in speed and intent. These dynamics challenge the quasi-static assumption underlying the optimization in Eq.(10), as computed solutions may already be outdated by the time they are applied. Evaluating controller performance in overground environments is therefore, an important direction for future work.

Lastly, the VFF controller assumes that the user has the same desired reference path for all speeds. However, joint trajectories vary with walking speed [18], [19], and they may also change with acclimatization to the exoskeleton. In the VFF control law, higher errors lead to corrective behaviour overriding assistive, which blocks assistive adaptation, and increased disagreement between the user and exoskeleton (correction involves disagreement by nature). It is possible that the participants who preferred the fixed controller, had different desired trajectories compared to the medium calibration speed, especially at slow speeds, causing unnecessary corrective torques and disagreements. Therefore, another area of further improvement includes both velocity and trajectory adaptation.

VI. Conclusion

The adaptive, modified VFF controller resolves the damping behaviour in the original controller and reduces the disagreement between user and the exoskeleton by modulating the desired joint velocities according to the sign of mechanical work. In an experimental study with 12 participants walking on a treadmill at $40 \pm 10\ \%BL/s$, the adaptive controller significantly reduced energy dissipation by the exoskeleton compared to the fixed controller while preserving corrective behavior and kinematics. Analysis of muscular effort and interaction torques using interaction portraits revealed that most participants co-adapted well to the adaptive controller, showing less disagreement with the device and more frequently leading the motion, particularly at higher speeds. Nonetheless, some participants preferred the steady, predictable behavior of the fixed controller, specifically for slow speed. Overall, these encouraging results suggest that optimizing energy transfer between the user and exoskeleton can improve walking speed synchronization by personalizing the velocity profile to each individual.

References

[1] M. Lotze, C. Braun, N. Birbaumer, S. Anders, and L. G. Cohen, "Motor learning elicited by voluntary drive," *Brain : a journal of neurology*, vol. 126, pp. 866–872, 2003.

[2] J. L. Emken, R. Benitez, and D. J. Reinkensmeyer, "Human-robot cooperative movement training: Learning a novel sensory motor transformation during walking with robotic assistance-as-needed," *Journal of NeuroEngineering and Rehabilitation*, vol. 4, no. 8, 2007.

[3] L. Marchal-Crespo and D. J. Reinkensmeyer, "Review of control strategies for robotic movement training after neurologic injury," *Journal of NeuroEngineering and Rehabilitation*, vol. 6, no. 20, 2009.

[4] R. Baud, A. R. Manzoori, A. Ijspeert, and M. Bouri, "Review of control strategies for lower-limb exoskeletons to assist gait," *Journal of NeuroEngineering and Rehabilitation*, vol. 18, no. 119, 2021.

[5] A. Duschau-Wicke, J. von Zitzewitz, A. Caprez, L. Lunenburger, and R. Riener, "Path control: A method for patient-cooperative robot-aided gait rehabilitation," *IEEE Transactions on Neural Systems and Rehabilitation Engineering*, vol. 18, no. 1, pp. 38–48, 2010.

[6] J. Lopes, C. Pinheiro, J. Figueiredo, L. P. Reis, and C. P. Santos, "Assist-as-needed impedance control strategy for a wearable ankle robotic orthosis," in *2020 IEEE International Conference on Autonomous Robot Systems and Competitions (ICARSC)*, 2020, pp. 10–15.

[7] T. Gurriet, M. Tucker, A. Duburcq, G. Boeris, and A. D. Ames, "Towards variable assistance for lower body exoskeletons," *IEEE Robotics and Automation Letters*, vol. 5, no. 1, pp. 266–273, 2020.

[8] A. Martínez, B. Lawson, and M. Goldfarb, "A controller for guiding leg movement during overground walking with a lower limb exoskeleton," *IEEE Transactions on Robotics*, vol. 34, no. 1, pp. 183–193, 2018.

[9] A. Martínez, B. Lawson, C. Durrough, and M. Goldfarb, "A velocity-field-based controller for assisting leg movement during walking with a bilateral hip and knee lower limb exoskeleton," vol. 35, no. 2, 2019, pp. 307–316.

[10] M. Sharifi, J. K. Mehr, V. K. Mushahwar, and M. Tavakoli, "Autonomous locomotion trajectory shaping and nonlinear control for lower limb exoskeletons," *IEEE/ASME Transactions on Mechatronics*, vol. 27, no. 2, pp. 645–655, 2022.

[11] N. Garcia-Hernandez, C. Munguia-Angeles, and V. Parra-Vega, "Assist-as-needed robotic strategy based on velocity fields for enhancing motor training," *IEEE/ASME Transactions on Mechatronics*, vol. 30, no. 2, pp. 1504–1513, 2025.

[12] M. Shushtari, J. Foellmer, and A. Arami, "Human–exoskeleton interaction portrait," *Journal of NeuroEngineering and Rehabilitation*, vol. 21, p. 152, 2024. [Online]. Available: https://jneuroengrehab.biomedcentral.com/articles/10.1186/s12984-024-01447-1

[13] R. Tibshirani, "Proximal gradient descent and acceleration," May 2015. [Online]. Available: https://stat.cmu.edu/ ryantibs/convexopt-S15/lectures/08-prox-grad.pdf

[14] S. Tan and J. Lu, "A nesterov's accelerated projected gradient method for monotone variational inequalities," 2022. [Online]. Available: https://arxiv.org/abs/2212.08346

[15] M. Shushtari and A. Arami, "Human–exoskeleton interaction force estimation in indego exoskeleton," *Robotics*, vol. 12, no. 3, p. 66, 2023. [Online]. Available: https://www.mdpi.com/2218-6581/12/3/66

[16] R. L. Lieber, T. J. Roberts, S. S. Blemker, S. S. M. Lee, and W. Herzog, "Skeletal muscle mechanics, energetics and plasticity," *Journal of NeuroEngineering and Rehabilitation*, vol. 14, no. 1, p. 108, 2017. [Online]. Available: https://jneuroengrehab.biomedcentral.com/articles/10.1186/s12984-017-0318-y

[17] C. A. Fukuchi, R. K. Fukuchi, and M. Duarte, "A public dataset of overground and treadmill walking kinematcis and kinetics in healthy individuals," *PeerJ*, vol. 6, p. e4640, 2018.

[18] ——, "Effects of walking speed on gait biomechanics in healthy participants: a systematic review and meta-analysis," *Systematic Reviews*, vol. 8, no. 153, 2019.

[19] J. Padulo, S. Rampichini, M. Borrelli, D. M. Buono, C. Doria, and F. Esposito, "Gait variability at different walking speeds," *Journal of functional morphology and kinesiology*, p. 158, 2023.